Eur. Phys. J. A (2016) **52**: 85
DOI 10.1140/epja/i2016-16085-2

THE EUROPEAN PHYSICAL JOURNAL A

Review

Data analysis in solar neutrinos liquid-scintillator detectors*

G. Testera[a]

INFN, Sezione di Genova, Via Dodecaneso 33, 16146 Genova, Italy

Received: 13 July 2015
Published online: 18 April 2016 –
Communicated by C. Broggini

Abstract. This paper focuses on the description of some of the methods developed to extract the solar neutrino signal from the background by the two running experiments (Borexino and Kamland) based on the use of a large volume of liquid scintillator.

1 Introduction

After the results of the radio-chemical experiments and the measurement of the high energy portion of the flux of ^{8}B solar neutrinos obtained by the water Cherenkov experiments, the next generation of real-time solar neutrino experiments aimed to detect the low-energy components (MeV or subMeV) of the solar neutrino spectrum. The use of large volume liquid scintillators is the only viable choice being the scintillation yield about 50 times higher than the Cerenkov one. Presently, two liquid-scintillator–based detectors have reported measurements of solar neutrinos: Borexino and Kamland.

Neutrinos with all the flavours undergo elastic scattering off the electrons in the scintillator target. In the energy range relevant for solar neutrinos the cross section is about 5–6 times higher for ν_e than for $\nu_{\mu,\tau}$. The solar neutrino signal is generated by the scintillation light produced by the energy loss of the recoiled electrons. The choice and the optimisation of the methods of analysis are driven by the need of identifying all the sources of radioactive (intrinsic and cosmogenic) background that can mimic the solar neutrino signal in absence of special signatures of the signal itself. In fact the emission of scintillation light is isotropic and any information about the initial direction of the incoming solar neutrinos is lost. On the contrary, the directionality is a powerful tool to discriminate between signal and background in water Cerenkov detectors. The shape of the energy spectrum of the recoiled electrons is the key signature of solar neutrinos in liquid-scintillator detectors. The expected interaction rate is of the order of only few tens or few counts/day 100 t (depending on the energy range) and this low rate sets the requirements about the level of the necessary background rate. Note that almost all the γ, β^+ and β^- originated in decays of radioactive isotopes fall in the energy region below few MeV. The α emitter are also dangerous since the light generated by heavily ionising particles like α of several MeV in liquid scintillator is roughly equivalent to that of an electron with ten time less energy.

Borexino has been especially designed to measure the flux of the mono energetic ^{7}Be neutrinos with $E = 0.862$ keV. It started the data taking in May 2007 and the first real time measurement of the interaction rate of the ^{7}Be neutrinos was obtained with the first 47.4 live days [1]. Later more precise measurements have been reported [2, 3] together with the studies of a possible day-night variation of the flux of ^{7}Be [4] and its seasonal modulation [5], the first measurement of the pep flux and the best limit of the CNO [6] and the real time measurement of the primary pp neutrinos [7]. Despite the low mass a measurement of the ^{8}B neutrinos in Borexino has been possible thanks to the low background: this was the first attempt to measure the interaction rate of ^{8}B ν in a liquid scintillator detector and to push down the energy threshold to 3 MeV [8].

Kamland was designed with the main goal of detecting anti-ν from reactors and its radioactive background resulted higher than the typical Borexino one. Kamland published its results about anti-ν from reactors in 2002 [9]. These results are of outstanding importance to select the range of the parameters explaining the solar neutrino oscillations. After completion of the primary goal in the reactor phase, Kamland went through major purification of the liquid scintillator from May 2007, with the goal of reducing the intrinsic radioactive background originating mainly mainly from ^{210}Pb and ^{85}Kr, and made a measurement of ^{7}Be solar neutrinos [10]. Before the purification Kamland reported results about ^{8}B [11] interaction rate with 5.5 MeV threshold.

Here we describe some selected features of the analysis procedures used in these two experiments. They have

* Contribution to the Topical Issue "Underground nuclear astrophysics and solar neutrinos: Impact on astrophysics, solar and neutrino physics" edited by Gianpaolo Bellini, Carlo Broggini, Alessandra Guglielmetti.

[a] e-mail: Gemma.Testera@ge.infn.it

Table 1. This table summarises some of the main features of Borexino and Kamland. More details are in [12], [9] and [13]. Here LC means Light Concentrators. PC is pseudocumene (1,2,4 trimethylbenzene), PPO is 2,5 diphenyloxazole, DMP is dimethylphthalate.

	Borexino	Kamland
Depth	3800 m.w.e	2700 m.w.e.
IV radius (m)	4.25	6.5
Scintillator mass (t)	278	10^3
SSS radius (m)	6.85	9
Inner PMTs	2212 8″ (371 with LC)	1879 (1325 17″ plus 554 20″)
Scintillator solvent	PC	80.2% dodecane, 19,8% PC
Scintillator fluor	PPO (1.5 g/liter)	PPO (1.5 g/liter)
Scintillator density	0.8802 g/cm^3 at 15 °C	0.780 g/cm^3 at 11.5 °C
Target electrons	$2.90 \cdot 10^{29}$ e/m^3	$2.67 \cdot 10^{29}$ e/m^3
Buffer liquid	PC+DMP (3 g/l)	dodecane and isoparaffin oil
OD PMTs	208 8″	225 20″

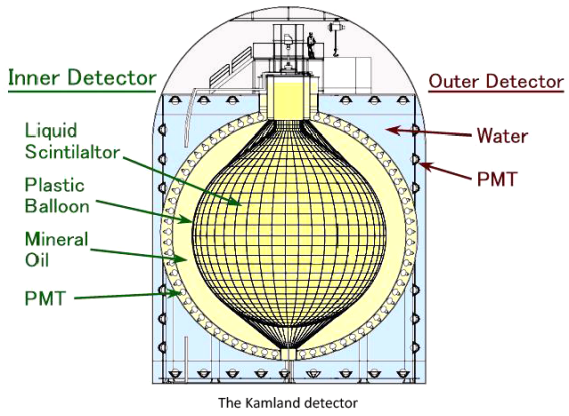

Fig. 1. The Kamland detector.

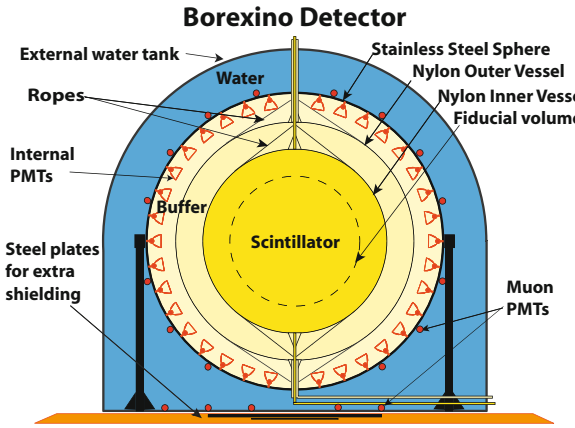

Fig. 2. the Borexino detector.

many common characteristics and the methods that they have developed represent a benchmark for any scintillator based low energy neutrino detector.

2 Brief description of Borexino and Kamland

Both the detectors are installed underground to reduce the muon flux. They are built using shells of materials with increasing radio-purity while moving from the outermost part to the innermost. The most stringent requirements concern the scintillator itself. Schematically the liquid scintillator (LS) is contained in a thin vessel (Inner Vessel-IV) immersed in another not scintillating liquid (buffer). The light is detected by photomultipliers (PMTs) mounted on a stainless steel sphere. The scintillator and these PMTs form the Inner Detector (ID) which is basically an unsegmented calorimeter. The sphere is contained within a cylinder filled by water and viewed by additional PMTs forming the Outer Detector (OD). The water is at the same time a shield against γ and neutrons and an active Cerenkov muon identifier.

Table 1 reports the main characteristics of the two detectors and figs. 1 and 2 show their scheme.

Most particle interactions in the ID of Borexino and Kamland other than muons produce less than one photoelectron per PMT. For each of them the quantities that are measured are the number of PMTs receiving an hit together with the associated charge (number of photoelectrons - phe) and the time of the hits. Details of the design of the electronics of the two experiments result in some differences between the information available for the analysis.

Both the detectors self trigger when a selected number of PMTs detect at least one hit within a given time interval. The discriminator thresholds are set to a fraction of the single phe signal (typically 0.15–0.2). Note that in Borexino the light yield is 500 phe/MeV and in Kamland is 300 phe/MeV if only the 17″PMTs are used while it is 500 phe/MeV is all the ID PMT are considered. The typical Borexino trigger threshold is set to 20–30 PMTs (it changed during the time) fired within 100 ns corresponding to about 60 KeV. The trigger conditions of Kam-

land changed during time but usually the energy threshold is higher: about 200 of the 17″ PMTs were required at the beginning of the data taking (corresponding to about 0.7 MeV). During the purification of the scintillator the threshold decreased and, after the purification,was set to 70 of the 17″ PMTs [14]. The trigger threshold goes to a lower energy for 1 ms after the primary trigger.

In Borexino each PMTs is connected to an electronic chain made by an analog part (providing amplification and integration of the signal) and a digital part with a fast discriminator for time measurements and ADC for digitising the integrated signal [12]. When a trigger is detected, an acquisition gate of 15 μs is opened and the times of all the firing PMTs are registered. The times of multiple hits on the same PMT are not detected when the time delay between two consecutive pulses is less than 140 ns. This dead time is software extended to 180 ns. Signals originated by a single energy deposit are identified by a software algorithm searching for clusters of hits. Multiple clusters in a single acquisition gate are expected in case of fast radioactive decay chains. The dead time between two consecutive gates is 2.5 μs. Following the detection of an hit in a given PMT, its signal is integrated for 80 ns thus measuring the number of photoelectrons arriving within this time interval.

In Kamland each PMT is connected to two Analog Transient Waveform Digitizer (ATWD) [14]. These devices have an array of capacitors maintaining the waveform in an analog form. If the PMT signal crosses the discriminator threshold, the ATWD starts to capture the PMT signal in 128 samples at the typical frequency of 0.65 GHz, resulting in about 200 ns of data in each waveform. The ATWD holds the waveform for 175 ns while awaiting for the global trigger decision, based on which the ATWD either erases the waveform within 1 μs or digitizes the waveform with a 10 bit ADC in 27 μs. To reduce the dead time, each PMT is connected to two ATWDs, so that one can acquire a waveform when the other is busy. After the pedestal and real sampling time for each ATWD have been characterised by using special dedicated runs, the pulse time and charge of each PMTs are extracted from the waveforms.

3 The analysis methods

Neutrino induced events in liquid scintillators are intrinsically indistinguishable on a event by event basis from the background due to α, β or γ decays.

There are basically three methods of analysis

– *Spectral fit.* The energy spectrum of the solar neutrino induced event is the signature which is used to distinguish it from the background. The interaction rates due to ^{7}Be, pep, pp neutrino an the limit on the CNO have been obtained through a fit of the binned energy spectrum of the events surviving a set of quality cuts. This approach requires a background model that is the identification of the spectral components of the background since the fit procedure can return only the amplitudes of the components included in the fit function. The χ^2 of the fit is used to decide if the model is acceptable. The fit procedure can be simple (using only the energy information) or multivariate. For the ^{7}Be and pp measurement the simple method has been used. The pep and CNO analysis performed by Borexino demanded more sophisticated multivariate fit due to the lower signal to background ratio than that of the ^{7}Be analysis. Details about the analysis procedures used in Borexino are in [5].
When possible, some background is removed from the spectra by applying statistical subtraction techniques based on the particle pulse shape identification. The statistical subtraction method has been used by Borexino to remove the α background due to the ^{210}Po decay.
– *Background subtraction.* The measurement of the interaction rate of ^{8}B in both Borexino and Kamland cannot be obtained by identifying signal and background based on their spectral shapes since the statistic is too low (particularly for Borexino). The analysis is based on the identification and evaluation of the background eventually followed by a unbinned fit.
– *Time variation analysis.* The search for the seasonal modulation (with about 7% amplitude) of the solar neutrino due to the change in time of the Earth to Sun distance could in principle be performed extracting the signal through a spectral fit of data collected in a period of the order of 1 month. Presently results about the ^{7}B have been reported by Borexino using three years of data. The spectral fit approach does not perform well with low statistic samples and alternative methods have been developed.

4 Position reconstruction and definition of fiducial volume

The ability to define a fiducial volume through the reconstruction of the position of the scintillation events is crucial to strongly suppress any external background in both the experiments. The two features that determine the success of the position reconstruction are the fast response of the organic liquid scintillator and the precision of the time measurement by the photomultipliers and the related electronics. The performances of the position reconstruction have been studied by both the experiments by comparing the true and reconstructed events position using radioactive calibration sources deployed in the scintillator [15, 16]. The accuracy of the position reconstruction directly influences the precision of the definition of the fiducial volume and thus the number of target electrons (needed to convert the measured interaction rate to the incoming neutrino flux).

The fiducial volume is usually defined based on the distance of the reconstructed point from the detector center. In Borexino, in the context of the search for the seasonal modulation of the ^{7}Be signal, a new approach has been developed in which the fiducial volume is defined as the set of points having a distance from the vessel wall larger than a given value. This definition is not equivalent to the previous one since the Borexino vessel showed significant

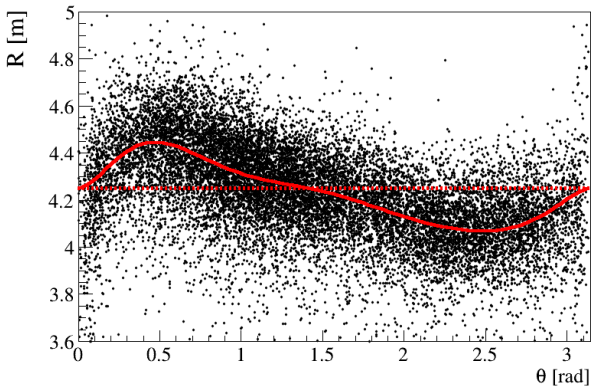

Fig. 3. $R-\theta$ ($R=\sqrt{x^2+y^2}$) distribution of the events in the energy region 800–900 keV in November 2007 used in Borexino for the IV shape reconstruction. The best fit vessel shape is shown in a solid red line. The dashed red line represents the nominal spherical vessel with $R = 4.25$ m.

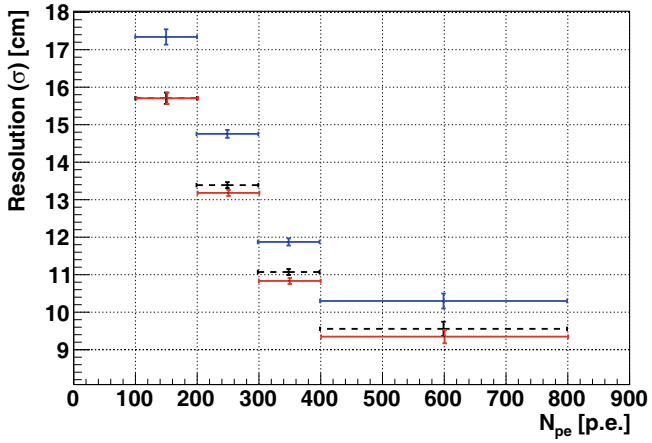

Fig. 4. The resolution of the x (solid red line), y (dashed black line), z (dotted blue line) coordinates as a function of energy measured in Borexino using the calibration sources.

deformation from a spherical shape. The real IV profile is determined on a weekly base by using background events reconstructed on the nylon surface with energy between 800 and 900 keV and identified as due to ^{210}Bi decay. Assuming azimuthal symmetry, the dependence of the reconstructed radius R on the θ angle is fitted with a 2D analytical function (red line) having a Gaussian width (see fig. 3).

4.1 Position reconstruction in Borexino

The position reconstruction algorithm used in Borexino determines the most likely vertex position $\boldsymbol{r}_0$ of the interaction using the arrival times t_i^j of the detected photons (labelled by the index i) on each PMT (labeled by j) and the position vectors $\boldsymbol{r}^j$ of these PMTs.

The algorithm subtracts from each measured time t_i^j a position-dependent photon travel time $T^j_{\rm travel}$ from the interaction point to the PMT j

$$T^j_{\rm travel}(\boldsymbol{r}_0, \boldsymbol{r}^j) = |\boldsymbol{r}_0 - \boldsymbol{r}^j| \frac{n_{\rm eff}}{c} \qquad (1)$$

and then it maximises the likelihood $L_E(\boldsymbol{r}_0, t_0 \mid (\boldsymbol{r}^j, t_i^j))$ that the event occurs at the time t_0 in the position $\boldsymbol{r}_0$ given the measured hit space-time pattern $(\boldsymbol{r}^j, t_i^j)$.

The maximisation uses a energy dependent probability density function of the hit detection. The quantity $n_{\rm eff}$ appearing in eq. (1) is called "effective refraction index" and it is used to define an effective velocity of the photons: it is a single parameter that globally takes into account the fact that photons with different wavelengths travel with different group velocity and that photons do not go straight from the emission to the detection points but they can be scattered or reflected. Its value is determined using the calibration data. The distribution of the differences between the true and reconstructed x and y coordinates is centered on zero and it has an rms of ~ 0.8 cm. Instead, the z coordinate shows a systematic shift of ~ 3 cm downwards with respect to the nominal position whose origin is unclear. Figure 4 shows the position resolution measured in Borexino.

4.2 Position reconstruction in Kamland

The algorithm used in Kamland finds the vertex iteratively [17]. It uses only the 17″ PMTs because of their better time resolution. The starting point $\boldsymbol{r}_{\rm start}$ is defined by a charge weighted average position

$$\boldsymbol{r}_{\rm start} = 1.62 \frac{\sum_j N^j_{pe} \boldsymbol{r}_j}{\sum_i N^j_{pe}} \qquad (2)$$

where j runs on all the pulses. The coefficient 1.62 is found using the calibration sources. A time t'_j representing the pulse time t_j minus the average photon travel time is defined by

$$t'_j = t_j - t_{{\rm travel},j} = t_j - \left(\frac{r^S_j c}{n^S_{\rm eff}} + \frac{r^B_j c}{n^B_{\rm eff}} \right), \qquad (3)$$

where we have introduced, as in Borexino, empirical effective refraction indexes. Note that here we have two values: one for the liquid scintillator $n^S_{\rm eff}$ and one for the outer buffer $n^B_{\rm eff}$. The ratio $n^B_{\rm eff}/n^S_{\rm eff}$ is found to be 0.89 [18]. Then the distribution of t'_j is built and its peak value $t'_{\rm peak}$ is found. The algorithm then defines $\delta\boldsymbol{r}$ as

$$\delta\boldsymbol{r} = \sum \frac{t'_j - t'_{\rm peak}}{t_{{\rm travel},j}} \cdot (\boldsymbol{r} - \boldsymbol{r}_j), \qquad (4)$$

where $\boldsymbol{r}$ is the current estimation of the event position. The procedure is iterated until a maximum number of steps is reached or δr is less than 1 mm. A vertex reconstruction status is associated to each event. As example of the performances fig. 5 shows the differences between

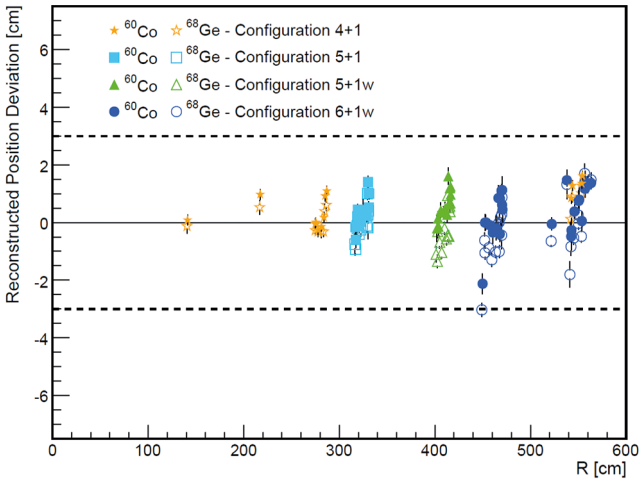

Fig. 5. Percent difference between reconstructed and true source position for various calibration sources deployed in Kamland. Details are in [16].

the true and reconstructed positions obtained with calibration sources. Data collected with the full volume calibration system showed reconstruction deviations less that 5 cm [10].

5 Energy reconstruction

The energy deposit in the scintillator (visible energy) is obtained from the number of photoelectrons or from the number of fired PMTs (energy estimators). The true event energy differs from the visible energy due to the non linear phenomenon of ionisation quenching [19] which affect electrons, γ- and α-induced scintillation in a different way, position dependent effects and others factors that must be correctly included. Establishing this relation between true energy and measured number of photoelectrons or hits is one of the key point in the analysis. The accuracy of the model of the energy response directly influences the accuracy of the measurement of the solar neutrino signal.

The ionisation quenching effect is related to the fact that the higher is the specific energy loss $\mathrm{d}E/\mathrm{d}x$ the lower is the number of scintillation photons $\mathrm{d}Y$ emitted per unit of path length $\mathrm{d}x$. For β^+ and β^- the following relation is used

$$\frac{\mathrm{d}Y}{\mathrm{d}x} = \frac{Y_0 \cdot \mathrm{d}E/\mathrm{d}x}{1 + kB \cdot \mathrm{d}E/\mathrm{d}x}\,, \tag{5}$$

where k_B is called the quenching parameter, and Y_0 is the scintillation yield in absence of quenching ($k_B = 0$). The total number of emitted photons Y_p is then related to the amount of deposited energy E through a non-linear relation:

$$Y_p = Y_0 \cdot Q_p(E) \cdot E \tag{6}$$

where $Q_p(E) < 1$ is called quenching factor.

The suffix p recalls that $Q_p(E)$ and Y_p depend on the particle type p (α, β, or γ). The quenching factor for β particles $Q_\beta(E)$ can be obtained by integrating $\mathrm{d}Y/\mathrm{d}x$;

$$Q_\beta(E) = \frac{1}{E}\int_0^E \frac{\mathrm{d}E}{1 + k_B \cdot \mathrm{d}E/\mathrm{d}x}\,. \tag{7}$$

In general, the amount of scintillation light emitted when a γ with energy E is fully absorbed by the scintillator is significantly lower than the amount of light emitted by an electron with the same energy E. In fact, the interactions of γ-rays in the scintillator are observed by detecting the sum of the scintillation light emitted due to the various electrons (and positrons) scattered (or produced) by the parent γ and depositing in the scintillator the energy E_i. The amount of scintillation light Y_γ generated by the γ is then obtained by summing over all the electron contributions i

$$Y_\gamma = Y_0 \sum_i E_i Q_\beta(E_i) \equiv Y_0 \cdot Q_\gamma(E) \cdot E. \tag{8}$$

The previous relation defines $Q_\gamma(E)$. Since $Q_\beta(E)$ decreases as a function of the energy, it results that $Q_\gamma(E)$ is smaller than $Q_\beta(E)$ for the same energy E. As a result, the quenching factor is not negligible for γ-rays with E in the MeV range.

The amount of Cherenkov light produced in liquid scintillators is expected to be at the level of few percent of the scintillation light yield and therefore not negligible. In addition the ultraviolet fraction of the Cherenkv light is absorbed by the scintillator and re-emitted at higher wavelengths.

5.1 Energy reconstruction in Borexino

In Borexino different energy estimators are defined. N_p is the number of fired PMTs within the cluster duration, N_h is the number of detected hit on the PMTs including multiple hits, N_{pe} is the number of photoelectrons defined as the sum of the individual PMT charges normalised to the charge of the peak of the single photoelectron response, N_{pe}^d is defined as N_{pe} but with the addition of the dark noise subtraction. These variables are properly normalised run by run to accounts for the varying number of active channels.

The energy response in Borexino is determined by two methods: one is based on a full Monte Carlo simulation and the other relies on analytical models. Both methods have been used for the ^{7}Be, pep and CNO analysis while for the pp one only the analytical has been used.

The Borexino Monte Carlo code is an *ab initio* simulation (based on the GEANT4 package) of all the processes influencing the energy deposit of each type of particle in the scintillator and in the materials building the detector. It is designed to reproduce the number of hits and photoelectrons and their time distribution on each PMTs for any type of energy deposit in every point of the scintillator. It models the scintillation and Cherenkov light emission, the light propagation processes including the scattering, absorption, re-emission and reflection, the

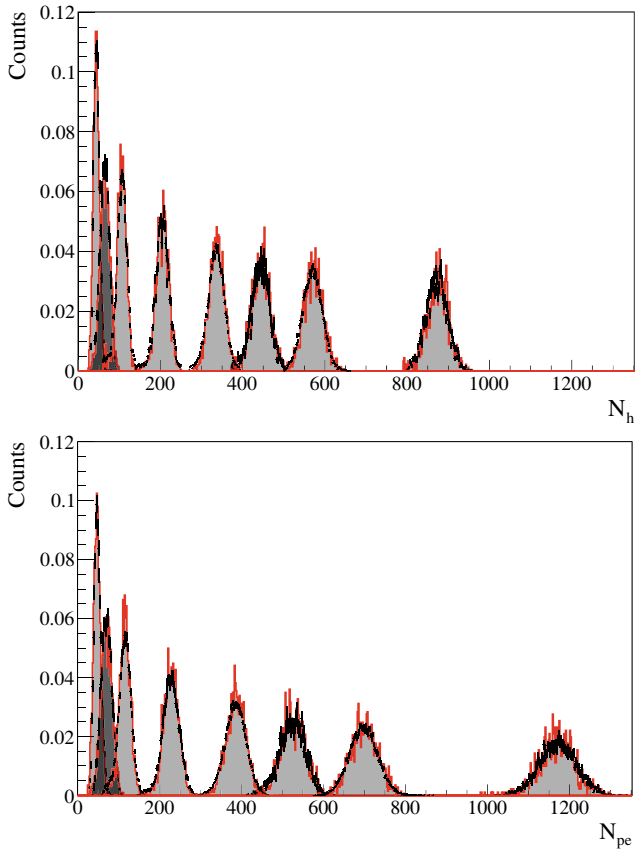

Fig. 6. Energy spectra (N_h and N_{pe}^d variables) of the calibration sources placed in the detector's center: measured data (black lines) *versus* the Monte Carlo simulation (areas dashed with red lines). The peaks represent (from the left to the right) the total γ decay energy of ^{57}Co, ^{139}Ce, ^{203}Hg, ^{85}Sr, ^{54}Mn, ^{65}Zn, ^{40}K, and ^{60}Co. A similar plot is obtained with the N_p estimator.

light detection and the electronics response. The scintillation photons are tracked one by one until they reach a PMT and are possibly detected or until they are absorbed elsewhere. The simulation reproduces the real distribution of active PMTs, the measured dark noise, the real gain and the shape of the single photoelectron response of each PMT following the run by run changes. It includes the simulation of the after pulses and of the measured transit time spread. γ sources deployed in the center of the detector have been used to tune and validate the Monte Carlo (see fig. 6) and to measure the quenching factor k_B. The value $kB = (0.0109 \pm 0.0006)$ cm/MeV has been obtained. ^{214}Po from a radon source deployed in several position in all the IV has been used to study the energy response as a function of the scintillation position. The same energy deposits occurring in various detector positions give rise to non-equal, position-dependent values of the energy estimators, N_h, N_p, and N_{pe}. This is due to the light absorption, the geometrical effects as for example the presence of the light concentrators mounted on some PMTs, the different response of individual electronics channels as well as non-uniform distribution of non-working electronics chains. The broken PMTs are concentrated close to

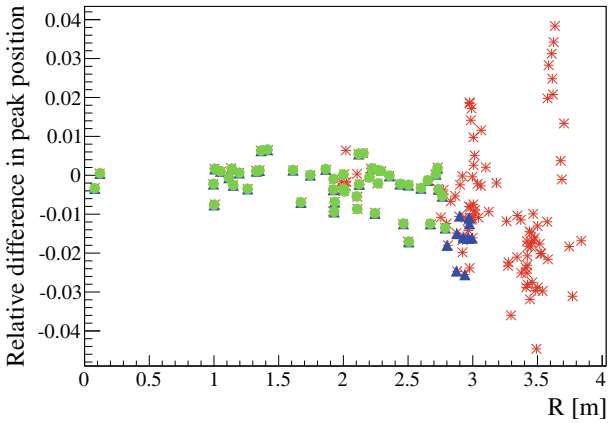

Fig. 7. The relative difference $\frac{N_h(MC)-N_h(data)}{N_h(data)}$ as a function of the radial position R of the ^{214}Po α peak from the radon calibration source. Blue triangles: ^{7}Be–ν FV, green circles: *pep*–ν FV, red stars: outside both FVs.

the bottom of the detector thus giving a higher light loss for off-center events in the bottom hemisphere with respect to the ones in the upper hemisphere. Figure 7 shows the percentage difference between the N_h peak position of the Monte Carlo and the data normalised to the data peak. The source locations within the FVs used for the *pep* and ^{7}Be neutrino analysis and locations outside both these FVs are shown in different colors.

To calibrate the detector energy response and the Monte Carlo is the energy region of interest for ^{8}B neutrinos (above 2–3 MeV) in Borexino it was used an ^{241}AmBe neutron source positioned at the center of the detector and at several positions at 3 m radius. Neutron capture on ^{1}H and on ^{12}C in the scintillator results in the emission of γ from the 2.223 MeV and 4.945 MeV excited states, respectively. In addition, neutron capture on the stainless steel of the insertion system produces γ-rays from the 7.631 MeV (^{56}Fe) and 9.298 MeV (^{54}Fe) excited states. The neutron capture time in Borexino is 256.0 ± 0.4. μs.

The analytical model has been developed to describe the relation between N_p, N_{pe} and N_{pe}^d and the particle energy. The quenching as a function of the electrons (or α) energy is parametrised through a formula. In case of γ the correct description of the quenching needs an additional free parameter or input from the Monte Carlo. The model describes the mean value of the energy estimator N_p, N_{pe}, N_{pe}^d averaged over the fiducial volume and its variance for uniformly distributed events:

$$N_{pe} = N_{pe}^0 + Y_0 \cdot E \cdot Q_p \cdot \overline{f_R(\boldsymbol{r})} = N_{pe} = N_{pe}^0 + Y_{det} \cdot E \cdot Q_p, \quad (9)$$

where Y_0 is the scintillator light yield, Q_p is the ionisation quenching factor and $f_R(\boldsymbol{r})$ is a geometrical factor non depending on the energy. The constant term accounts for the dark noise and it is absent in the model of N_{pe}^d. Y_{det} is defined by $Y_{det} = Y_0 \cdot \overline{f_R(\boldsymbol{r})}$.

The second ingredient of the model deals with the variance $\sigma^2_{N_{pe}}$ and the third central moment $\kappa_{N_{pe}}$. They can be computed starting from the corresponding individual

quantities associated with the multiplication process in the photomultiplier considering also the effect of the unavoidable dis-uniformity throughout the fiducial volume as described in details in [5]. The distribution function of N_{pe} is modelled as generalised gamma function while a Gaussian has been used for N_{pe}^{d}. In a similar way a model is developed for the number of fired PMTs N_p assuming that the distribution of the number of the triggered channels for events in the center obeys the binomial distribution. An analytical description pf N_h is not developed due to the difficulties introduced by multiple hits.

5.2 Energy reconstruction in Kamland

In Kamland once the position of the event is reconstructed it is used as input to the energy reconstruction algorithm [20]. The energy algorithm uses the pattern of hit and not-hit PMTs and the amount of charge collected by the hit PMTs to determine the visible energy of the event. The fact that a PMT does not register a hit in an event gives almost as much information about the energy as a hit PMT. In this way the information available to the energy reconstruction is maximised. The algorithm uses a maximum likelihood fit to obtain the visible energy E_{vis} given the distribution of charge q_i in the detector. The likelihood function $\ln L(E_{vsi}) = \sum_{PMTs} \ln(L_i(E_{vis}, q_i))$ is assembled from the likelihood of the individual PMTs. If the PMT has not detect an hit it contributes to the likelihood with $L_i(E_{vis}, q_i) = \exp(-\mu_i)$ while when the hit is detected its contribution is

$$\ln L(E, q_i) = \sum_{n=1}^{\infty} \frac{\mu_i^n \exp(-\mu_i)}{\mu_i!} P(q_i|n), \qquad (10)$$

where $P(q_i|n)$ is the probability (assumed Gaussian) that the charge q_i corresponds to n photoelectrons. μ_i is the mean expected number of photoelectrons on the PMTs i and it is given by

$$\mu_i = \eta_i E G(r_i, \theta_i, z_i) + \delta_i. \qquad (11)$$

The geometrical factor, G is normalised to the center. It accounts for exponential attenuation of the light with an average attenuation length of 30 m, the solid angle and others geometrical corrections modeled with a Monte Carlo code. The real energy E of the interacting particle is related to the reconstructed energy E_{vis} through

$$E_{vis} = E \cdot a_0 \cdot (1. - \delta_B(K_B, E) + k_c \delta_c(E) + k_0 \delta_0(E)), \qquad (12)$$

where the first factor in parenthesis accounts for the non linear ionisation quenching described by the Birks parameter k_B, $k_c\delta_c(E)$ accounts for Cerenkov light and $k_0\delta_0(E)$ keeps track of the energy that is lost in simulation due to particles dropping below the tracking threshold. a_0 is a normalisation obtained with the calibration data. Figure 8 shows the percent difference between reconstructed and true energy for various calibration sources as a function of the radial position.

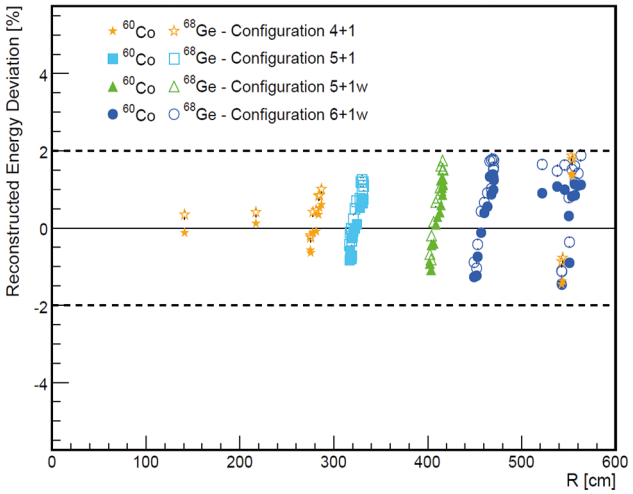

Fig. 8. Percent difference between reconstructed and true energy for various calibration sources deployed in Kamland. Details are in [16].

The energy resolution was studied using calibration sources: it is $7.4\%/\sqrt{E(\mathrm{MeV})}$ is only the 17″ PMTs are used and $6.5\%/\sqrt{E(\mathrm{MeV})}$ including all the PMTs [21].

6 Muon identification and track reconstruction

The only relevant component of cosmic radiation penetrating underground at the location of the Borexino or Kamland is due to muons. As example, at the Borexino depth, the muon flux is reduced to $1.2/(m^2h)$. Due to their mean energy close to 300 GeV, most muons travel through the detector without any significant loss of energy. Muons passing through the IV create a very large light output as they deposit hundreds of MeV of ionization energy. They are easily identified unless they cross the IV near the border and then their energy deposit could fall in the region of interest for solar neutrinos. The situation changes for muons crossing the buffer without touching the IV. Buffer muons generate light partly by the Cherenkov effect and partly by the residual scintillation of the buffer liquid. The light output is low enough to mimic a solar neutrino signal. Muons crossing only the water buffer are not dangerous.

Muons are identified in Kamland as events with more than 10^4 phe or events with more than 500 phe showing at least 5 firing PMTs in the outer detector [21].

In Borexino, for the muons crossing the ID, it is observed that their typical pulses feature longer rise and decay times than neutrino-like scintillation events of comparable energy. In addition, the number of detected photons is several orders of magnitude above the usual light output of point-like events, prolonging the signal substantially by generating large amounts of PMT after pulses. In Borexino tags for muons [22] based on the value of the peak and mean of the time distribution have been

developed. The inefficiency of this tag is evaluated to be $(1.0\pm0.2)\cdot10^{-5}$ [8]. After including also the muon identification by the OD the residual number of untagged muons in Borexino is estimated as $4.5 \pm 0.94 \cdot 10^{-4}\mu/(\text{day } 100\,\text{t})$ above 5 MeV. Details are in [22].

Muons produce unstable nuclei by spallation processes along their trajectory through the scintillator and the decay of such nuclei can mimic the solar neutrino signal. For short-lived radioisotopes, it is usually sufficient to veto all events following a muon for a duration corresponding to several half-lifes of the given isotope. However, when the half-life of the dangerous nuclei is longer, the induced dead time can become very large. To overcome this problem, the veto of events can be applied only to a cylindrical region around the muon track instead of the whole detection volume.

Tracking algorithms have been developed by both the experiments. In Borexino two independent tracking algorithms are combined. The OD tracking is based on the identification of the entry and exit points of the muons generated by the Cherenkov cone in water. The ID tracking relies on the distinctive photon arrival time pattern created by the scintillation light front emitted by the muon track. The results of both ID and OD tracking algorithms are later combined in a best fit global tracking. The parameters entering the tracking algorithms were tuned using a MC simulation of muon events. The evaluation of the accuracy of the tracking instead is performed on real data. Complete tracks with both entry and exit point are found for 98.5% of all muon events for the OD tracking. The global tracking algorithm returns a fitted track in 96.4% of all muon events. The angular resolution of the tracking was determined by utilising muon events, generated in the rock upstream of Borexino by the neutrinos of the CNGS beam flying from CERN to G. Sasso. The ones crossing both Borexino and the OPERA detector mounted in the same experimental hall have been selected. A track-by-track comparison between the two experiments returned a resolutions of 3° for OD/global tracking and 5° for ID tracking. In addition an external muon tracker mounted on top of Borexino was used. The lateral resolution (perpendicular to the muon track) can be derived from a track-by-track comparison with OPERA, returning a resolution of 40–50 cm (35 cm for muons crossing the IV).

Similarly in Kamland the muon track is reconstructed from the time of the of the first-arriving Cherenkov or scintillation photons at the PMT. Since for relativistic muons the wavefront of the scintillation light proceeds at the Cherenkov angle, and since muons generate enough light to generate photoelectrons in every PMT, by restricting the fit to the first-arriving photons both Cherenkov and scintillation photons can be treated identically. The observed muon track is then established by minimizing time-of-flight deviations from hypothetical muon tracks. The fit converges for 97% of all ID muon events. The majority of the events that are not re-constructed are believed to be multiple muons or muons accompanied by large electromagnetic or hadronic shower. Figure 9 shows the distribution of the muon track lengths in Kamland.

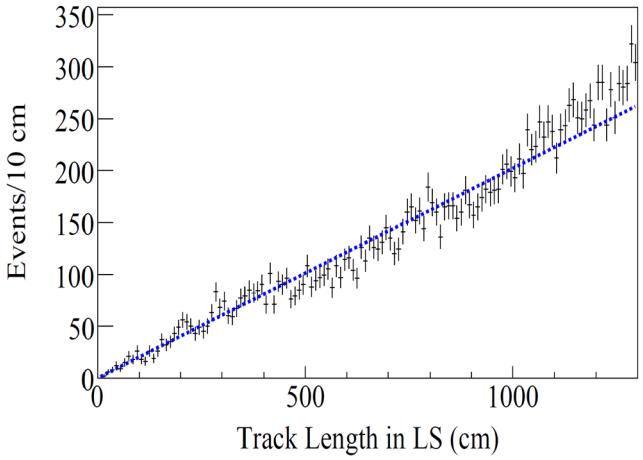

Fig. 9. Distribution of muon track lengths in the Kamland liquid scintillator. The dashed blue line shows the expected linear distribution for a sphere of nominal volume, and the average track length in this case is 867 cm. The average muon track length measured in the detector is 878 cm, in agreement with the expected value of 874 ± 13 cm. Figure taken from [21].

7 Fit of the energy spectra

7.1 Background model

Background events can be of four types.

- *External background*: it is mainly due to γ-rays emitted by the materials used in the construction of the detector or surrounding it. In Borexino the dominat contribution is due to the PMTs. It is strongly suppressed by the fiducial volume cut.
- *Surface background*: it is due to contamination of the vessel. It is alos suppressed by the fiducial volume cut. It is used in Borexino to define the real shape and position of the vessel as a function of time.
- *Internal background*. This is the most important one and it is due to the radioactivity of the scintillator: Many radioactive isotopes are common to Borexino and Kamland even if their specific activities are different. Figure 11 shows the solar neutrino signal and background components. Their rates are the ones determined in Borexino.
  Both the detectors observed a significant contamination of ^{210}Po. Its emitted α particle produces a peak lying in the energy region of the electrons scattered by the ^{7}Be neutrinos. Also a contamination of ^{210}Bi is observed. It is assumed that it is continuously originated by a contamination of ^{210}Pb not directly visible due to its very low Q (63 keV) value. ^{210}Bi decays by β^- toward ^{210}Po but the relative amounts of the two isotopes shows that they are out of equilibrium: there is much more ^{210}Po than that expected from the corresponding ^{210}Bi. ^{210}Bi is the most serious source of background for the pep and mostly for the CNO analysis. Both Borexino and Kamland observed that the ^{210}Bi may vary in time and space possibly due

Table 2. Summary of the data analysis conditions and results for the solar ^{7}Be neutrino measurement in Borexino and Kamland. The main sources of uncertainties are reported. The quoted errors included also the smaller contribution not listed here. The reported rates refer to the whole energy spectrum without cuts. For Kamland we report the background rate obtained in the whole fiducial volume and, in parenthesis, the value obtained in the region classified as rank-1 which is the cleanest. P_{ee} is the electron neutrino survival probability [5].

	Borexino	Kamland
Fit energy region (MeV)	0.25–1.6	0.5–0.8
FV cut (m)	$r < 3.021$, $\|z\| < 1.67$	$r < 4.5$
FV mass (t)	75.47	268.6
Exposure kt · d	56.06	165.4
Period	May 16th, 2007–May 8th, 2010	April 7th, 2009–June 21th, 2011
^{7}Be cpd/100 t	46.0 ± 1.5 (stat)$^{+1.5}_{-1.6}$ (syst)	58.2 ± 9
^{85}Kr cpd/100 t	31.2 ± 1.7 (stat) ± 4.7 (syst)	85.8 ± 5.9 (45.3 ± 10.2)
^{210}Bi cpd/100 t	41.0 ± 1.5 (stat) ± 2.3 (syst)	2397.4 ± 88.3 (395.5 ± 23.8)
^{40}K cpd/100 t	–	18.1 ± 2.9 (0.30 ± 3.8)
^{11}C cpd/100 t	28.5 ± 0.2 (stat) ± 0.7 (syst)	97.3 ± 1.0
FV error %	$^{+0.5}_{-1.3}$	3.4
Fit method error %	2.0	
Energy response %	2.7	7.9
Total systematic error %	$^{+3.4}_{-3.6}$	9.1
Total stat error %	3.3	12.4
862 keV ν_e equivalent flux (cm^{-2} s^{-1})	$2.78 \pm 0.13 \cdot 10^{9}$	$3.26 \pm 0.50 \cdot 10^{9}$
P_{ee}	0.51 ± 0.07	0.66 ± 0.14

to the release of contaminants from the IV. An interesting method of analysis has been developed by Kamland [10] to properly weight in the spectral fit the regions of the detector with a ^{210}Bi activity which differ each other by more than a factor 6. ^{85}Kr is another important source of background since its decay spectrum overlaps the electron recoiled spectrum induced by the interaction of ^{7}Be solar ν.

– *Cosmogenic background*. A time veto 300 ms long was used in Borexino for the ^{7}Be, pp, pep and CNO analysis. The residual rate is well below 1 cpd/100 t. Kamland used a 2 ms long veto in the ^{7}Be analysis. A special case is ^{11}C discussed later. For the ^{8}B analysis a deep study of the cosmogenic background was needed.

7.2 Fit methods

In all the approaches the binned energy spectra are fitted leaving the amplitude of the background and neutrino signals as free parameters. Some constraints are included for particular components. In Kamland the energy scale is determined through the calibration sources and the abovementioned amplitudes are the only free fit parameters. The same is true in case of Borexino when the Monte Carlo approach is used being the spectra of each component obtained through the Monte Carlo by generating events in all the scintillator volume following the behaviour in time of the detector and reconstructing them in the fiducial volume as for the data. When the analytical approach is used in Borexino there are additional free fit parameters: the averaged detector light yield Y_{det} defined in the relation 9, 4 parameters describing the response function and its variance, the position of the ^{210}Po peak and the starting point of the ^{11}C spectrum.

Organic liquid scintillators have a different time response for electrons and for α particles and, using the distribution of the measured PMT time signals, suitable parameters allowing α β discrimination are defined [5]. In Borexino the pulse shape discrimination has been used on an event-by-event basis defining cuts that remove some (but not all) α background but keep all the β. In addition it has been used with success to statistically subtract the ^{210}Po peak from the spectrum. The statistical subtraction is based on fitting the distribution of the α-β discrimination parameter in each energy bin by the sum of the one belonging to α and the one belonging to β. Then the energy bin content is replaced only with the resulting amplitude of the β parameter.

The ^{7}Be measurement has been reported by both Borexino and Kamland. Table 2 summarizes the main results about the ^{7}Be neutrinos obtained by the two experiments, the conditions of the analysis, the resulting background rates and the main sources of uncertainty. In Borexino the spectrum after the cut is fitted with and without statistical subtraction of the ^{210}Po, both using the analytical and Montecarlo methods. The fit has been performed using

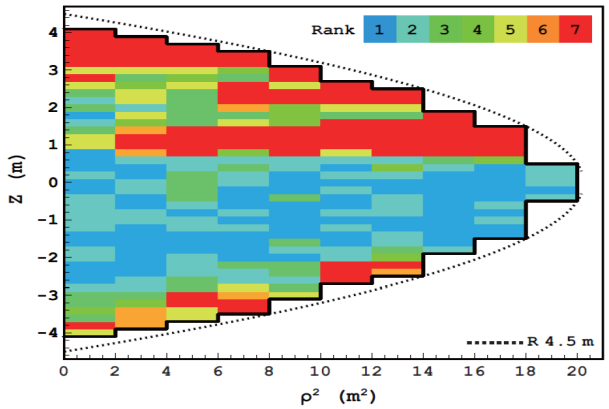

Fig. 10. Example of partition of the fiducial volume of Kamland into region with different ^{210}Bi contamination. Rank 1 is the cleanest with $< 5\,\mu$Bq/m^3. Rank 2, 3, 4, 5, 6 have activity in the ranges (5–10), (10–15) (15–20) (20–25) (25–30) μBq/m^3. Rank 6 has $> 30\,\mu$Bq/m^3. The figure is taken from [10].

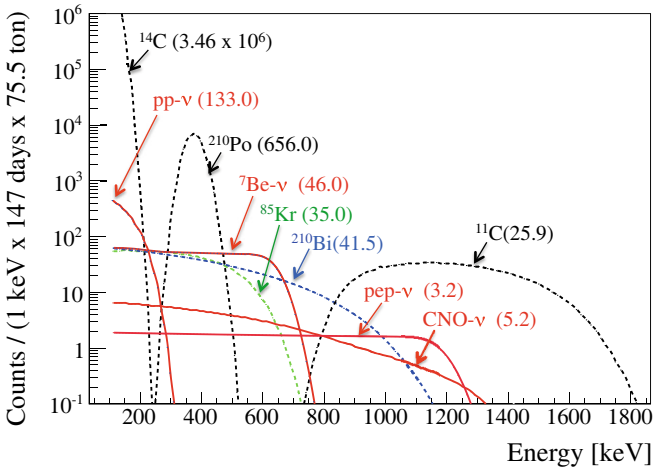

Fig. 11. The energy spectra of solar neutrinos and of the main background components. The realistic Borexino energy resolution is included. The rates are fixed at the values shown in parenthesis given in units of cpd/100 t.

the N_p, N_h and N_{pe}^d energy estimators. The differences among the results are included in the systematic error.

Kamland has developed a method to classify regions in the fiducial volume on the basis of an estimation of the ^{210}Bi count rate. A rank is assigned to them according to their background rate. Separate spectra are build for each rank and they are simultaneously fit to get the ^{7}Be solar neutrinos rate. An example of these regions is in fig. 10.

7.3 ^{11}C subtraction and multivariate analysis

The measurement of the pep solar neutrino interaction rate has been reported by Borexino only who provided at the same time the strongest limit to —date on the CNO solar neutrino interaction rate [6]. Figure 11 helps to understand that the pep measurement demanded the development of novel techniques for the rejection of ^{11}C cosmogenic background dominating 1–2 MeV energy region and to extend the procedure used for the ^{7}Be analysis. A multivariate fit which includes the energy spectrum, the radial distribution of the events and a proper defined pulse shape parameter useful to subtract the residual contribution of ^{11}C has been in fact adopted. The energy spectra before and after the ^{11}C subtraction have been fitted simultaneously.

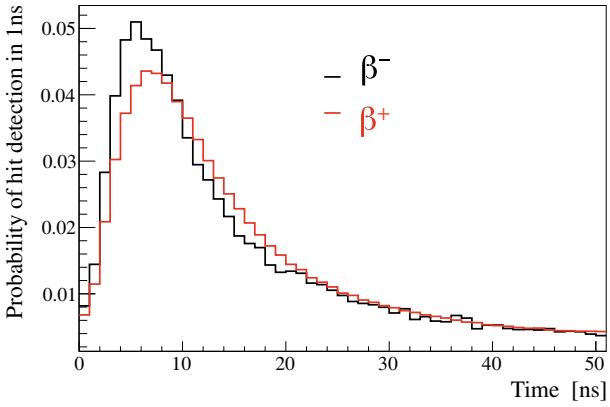

Fig. 12. Reconstructed photon emission times relative to the start time of the event: ^{214}Bi (β^-) events with $425 < N_h < 475$ identified by a ^{214}Bi-^{214}Po fast coincidence tag (black) and ^{11}C (β^+) events tagged by the TFC (blue).

^{11}C (a β_+ emitter with a mean life of 29.4 min) is continuously originated by the interaction of muons in the scintillator and cannot be removed by any purification procedure. The production of ^{11}C is accompanied by prompt neutrons and by the delayed 2.23 MeV γ ray resulting from the subsequent neutron capture in hydrogen. The TFC algorithm vetoes space-time regions of the detector after muon plus neutron coincidences in order to exclude the subsequent ^{11}C decays.

The TFC procedure can be summarized as follows:

- A suitable time veto have been applied at the beginning of each run, since muon plus neutron coincidences can be lost in the interval between runs.
- A veto of 2 hours is applied after muons with high neutron multiplicity.
- When the reconstructed neutron position is not reliable, due to the electronics saturation effects and/or due to a large fraction of noise hits, a cylindrical veto along the parent muon track with a radius of 80 cm for a time span of 2 hours is applied.
- If neutron clusters are found after the muon, then the cylindrical veto along the muon track described above is applied.
- A cylindrical veto is also applied around those muons tracks identified by the external detector only after which we find at least one neutron.
- If a neutron is found and its position is considered reliable, we veto a sphere of 1 m radius centered in this reconstructed position for 2 hours. Moreover, another 1 m spherical veto is applied around the point on the muon track that is closest to the neutron capture position.

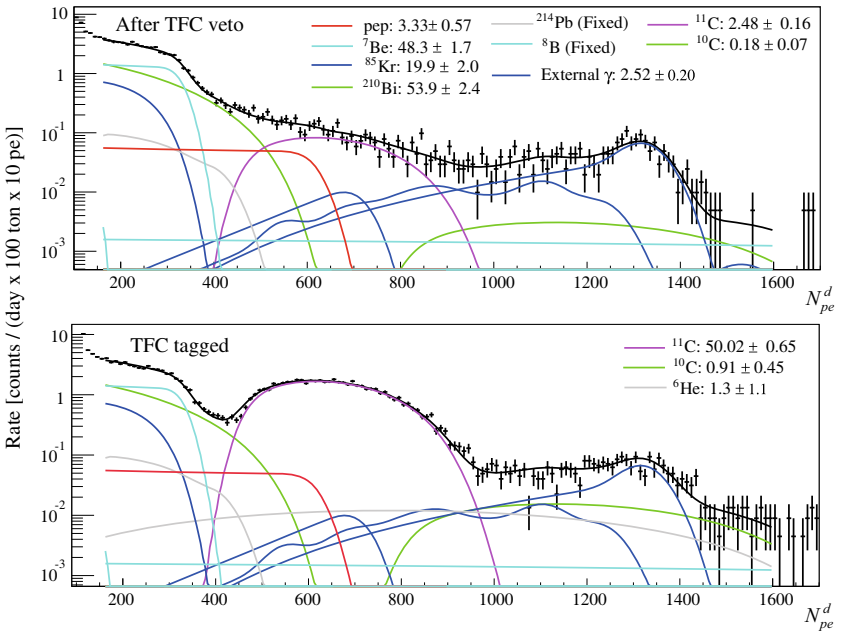

Fig. 13. Energy spectra and example of fit results performed on the N_{pe}^{d} energy estimator in the pep and CNO neutrino analysis. The top panel shows the best fit to the TFC–subtracted spectrum, while the bottom presents the fit to the complementary, TFC–tagged events. The best–fit values for the rates of the species included in the fit are shown in the legend in the units of cpd/100 t. The effect of the TFC procedure appears comparing the top and the bottom figure. The pep neutrinos interaction rate is 3.1 ± 0.6 (stat) ± 0.3 (syst) cpd/100 t. The CNO rate is < 7.9 cpd/100 t at 95% CL.

The application of this TFC algorithm results in $> 89.4\%$ ^{11}C rejection with a residual exposure of 48.5%. The ^{11}C rate decreases from ~ 28 cpd/100 tons to ~ 2.5 cpd/100 tons with a 51.5% loss of exposure.

The residual amount of ^{11}C is determined using a novel pulse-shape discrimination technique defining (within the framework of the Boost Decision Tree Algorithm) a parameter called (BDT parameter) with a discrimination power between β^- and β^+ induced scintillations.

In Borexino it is observed that the profile of the reconstructed emission times for scintillation photons produced by positron is different than those from electrons (see fig. 12). The difference is attributed to the formation of ortho-positronium that in a liquid medium can survive for few ns before annihilation [23].

This delay of the annihilation introduced by the ortho-positronium formation is comparable in size to the fast scintillation time constant of Borexino and introduces a measurable distortion in the time distribution of hit PMTs with respect to a pure β^- event (see fig. 12). Using a Boosted Decision Tree algorithm a pulse discrimination variable has been defined and its distribution has been included in the multivariate fit.

The multivariate fit approach is based on the maximisation of the "*total*" binned likelihood function $L_T(\boldsymbol{\theta})$, which depends on a set of parameters generically indicated by $\boldsymbol{\theta}$ and is a product of four factors:

$$L_T(\boldsymbol{\theta}) = L_e^{TFC_{\rm sub}}(\boldsymbol{\theta}) \cdot L_e^{TFC_{\rm tagged}}(\boldsymbol{\theta}) \cdot L_{\rm BDT}(\boldsymbol{\theta}) \cdot L_{\rm Rad}(\boldsymbol{\theta}), \quad (13)$$

where $L_e^{TFC_{\rm sub}}(\boldsymbol{\theta})$ is the likelihood function of the energy spectrum obtained after applying the TFC method to reduce the ^{11}C content; $L_e^{TFC_{\rm tagged}}(\boldsymbol{\theta})$ is the likelihood of the complementary energy spectrum containing events tagged by the TFC; $L_{\rm BDT}(\boldsymbol{\theta})$ is the likelihood of the $PS-BDT$ parameter, and finally $L_{\rm Rad}(\boldsymbol{\theta})$ refers to the likelihood of radial distribution of the events. The last factor is important to find the contribution of the external background whose rate is exponentially increasing with the distance from the center. Details about the single factors building the likelihood are in [5]. Figure 13 shows the result of the fit obtained using the estimator N_{pe}^{d} and the analytical approach for the description of the response function. Consistent results have been obtained using the Monte Carlo approach and the energy estimator N_h.

7.4 Low energy spectral fit

The most recent results about solar neutrinos is the first measurement of the pp neutrinos with a real time detector performed by Borexino. The pp spectrum ends at 420 KeV yielding a maximum electron recoil energy of 264 keV well above the typical Borexino threshold. The expected interaction rate is 133 cpd/100 t but the most part of them are in a energy region where the decay rate of ^{14}C is dominant. However the end point of ^{14}C (156 keV) is lower than the end point of the electron scattered by pp neutrinos. A purification campaign of the scintillator performed after the measurements described before has almost completely suppressed the ^{85}Kr and reduced the ^{210}Bi. This background reduction has allowed to single out an energy region in which the contribution of pp neutrinos can be detected (see fig. 14).

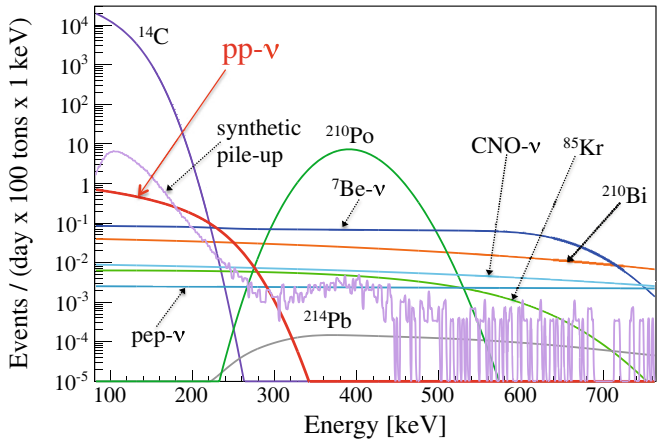

Fig. 14. Energy spectra of pp and all the radioactive background components with the amplitude determined by the fit which allows the pp measurement.

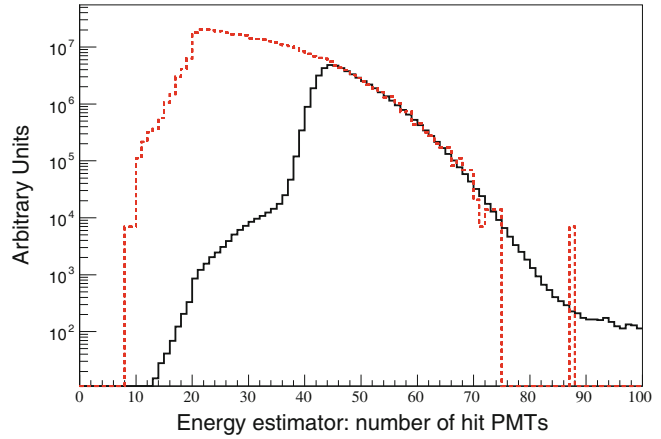

Fig. 15. The black curve is low-energy spectrum of Borexino events generating a trigger. The red plot is the spectrum of the second event in the acquisition gate following the one who has generated the trigger. Its spectrum extends without distortions until very low energies and it allows to determine the ^{14}C rate in a way independent of the main spectral fit.

The data used for this analysis were acquired from January 2012 to May 2013 (408 days of data in the so-called Borexino Phase II period). The data cuts are the same of ^{7}Be analysis excluding some soft α-β cut. The energy estimator that was used is the number of hit PMTs modeled through the analytical approach. The energy resolution is about 10% at 200 keV.

The ^{14}C rate was determined in a way independent from the spectral fit by fitting the spectra of the second cluster of events collected within the 16 μs acquisition gate. The spectrum of these events (see fig. 15) extends to a very low energy (limited only by the performances of the cluster algorithm) since the trigger is generated by the first event. The low energy part of this spectrum is basically only due to ^{14}C events. From the fit it is obtained a ^{14}C activity of 40 ± 1 Bq per 100 t. The corresponding ^{14}C/^{12}C isotopical abundance is $(2.7 \pm 0.1) \cdot 10^{-18}$ g/g. Figure 15 show the spectrum of ^{14}C in the first and second cluster. The second important contribution to the count rate in the energy region close to the end point of the pp induced spectrum is due to the so called pileup spectrum. These are events so close in time that they cannot be separated by the cluster algorithm and they are considered a single events. The rate and spectral shape of these events have been studied using a data driven method in which real data without any trigger selection cuts are artificially overlapped with random data samples. These combined synthetic events are selected and reconstructed using the procedure applied to regular data. A fit of synthetic pile-up with an analytical function gives 154 ± 10 cpd/100 t.

The spectra of other identified backgrounds are almost flat in the energy region of interest. The signal and background component in the low energy region are shown in fig. 14. The fit has been performed with the analytical method in the energy region 165–590 keV (60–220 N_p) after selecting the data using the same fiducial volume of the ^{7}Be analysis. ^{14}C, pileup and the rate of ^{7}Be solar neutrinos were constrained, pep and CNO were fixed, while the position of the ^{210}Po peak, the rate of ^{210}Po, ^{210}Bi, ^{85}Kr and pp were free.

The systematic uncertainty have been studied in a way similar to that used in Borexino for the other solar neutrinos analysis that is varying the fit conditions namely the fit energy range, the synthetic-*versus*-analytic pile-up, the spectral shape, and the energy estimator. The distribution of the results is peaked around the value of 144 cpd/100 t. The final result is 144 ± 13 (stat) ± 10 (syst) cpd/100 t to be compared with the expected value of 131 ± 2 cpd/100 t. From the χ^2 profile the absence of pp signal in the data is exclude at 10 σ level.

8 Background subtraction analysis and the ^{8}B flux measurement

^{8}B solar neutrinos are measured with high statistic by the water Cerenkov detectors. However, despite of the smaller active mass, a liquid scintillator detector can probe the ^{8}B solar ν spectrum with lower energy threshold. The lowest energy threshold of 3 MeV (electron recoil) has been achieved by Borexino. The value is determined by the count rate of γ from the external background particularly the ones of ^{208}Tl with 2.6 MeV energy. Due to the finite energy resolution they give a contribution also at higher energies. The measurement of ^{8}B solar neutrinos was reported by Kamland too with a 5.5 MeV threshold imposed to reject the background of ^{208}Tl ($Q = 5$ Mev) due to the residual ^{232}Th contamination of the scintillator. The radiopurity of the scintillator of Borexino makes the contribution of this internal background negligible. The expected ^{8}B solar neutrinos event rate is so low (it is 0.25 counts/day 100t for $E > 3$ MeV and about one half of this value for $E > 5$ MeV) for both the experiments (particularly for Borexino) that an analysis similar to the one performed for the ^{7}Be flux is impossible. Table 3 summarises the data-taking conditions of the two experiments while tables 4 and 5 show the residual background in Borexino

Table 3. Summary of the data analysis conditions and results for the ^{8}Be measurement in Borexino and Kamland.

	Borexino	Kamland
Energy threshold (MeV)	3	5.5
FV cut (m)	sphere $r = 3$	cylinder $r = 3$, $h = 6$
FV mass (t)	100	137.6
Exposure after the cuts kt · d	34.53	123
Period	July 15th, 2007–Aug 23th, 2009 (488 days)	April 7th, 2002–April 21th, 2007 (1432 days)

Table 4. Summary of the background above 3 MeV after the cuts in Borexino in the data sample used for the ^{8}B analysis.

Background	Rate (10^{-4} cpd/100 t)
Muons	4.5 ± 0.9
Neutrons	0.86 ± 0.0
External Background	64 ± 2
Fast cosmogenics	17 ± 2
^{10}C	22 ± 2
^{214}Bi	1.1 ± 0.4
^{208}Tl	840 ± 20
^{11}Be	320 ± 60

Table 5. Summary of the background after the cuts in Kamland [11] in the data sample used for the ^{8} analysis.

Background	Rate (10^{-4} cpd/100 t)
^{11}Be	724 ± 15
^{8}Li	166 ± 3
^{8}B	894 ± 2
Spallation other	3 ± 5
External γ-rays	205 ± 10
^{8}B CC on ^{13}C GND	47 ± 11
Reactor anti ν_e	13 ± 0.8
^{8}B CC on ^{13}C GND	8.9 ± 3.2
hep elastic scattering	4.9 ± 0.8
Atmospheric μ	16 ± 16

and Kamland after the cuts. Figures 16 and 17 plot the results.

The analysis is performed identifying and evaluating all the source of background and find the signal by subtraction. Kamland compared the results with that obtained with a unbinned likelihood fit of the energy spectra.

The main background for ^{8}B solar neutrinos in a liquid scintillator detector is due to the short and long lived cosmogenic isotopes produced by the interaction of muons with ^{12}C of the scintillator. The resulting isotopes often are accompanied by neutrons. They are listed in table 6. The ones relevant for Kamland are ^{8}Li, ^{8}B, ^{11}Be. In Borexino also the contribution of ^{10}C must be accounted. Cosmogenic isotopes with lifetime shorter than 2 s are reject

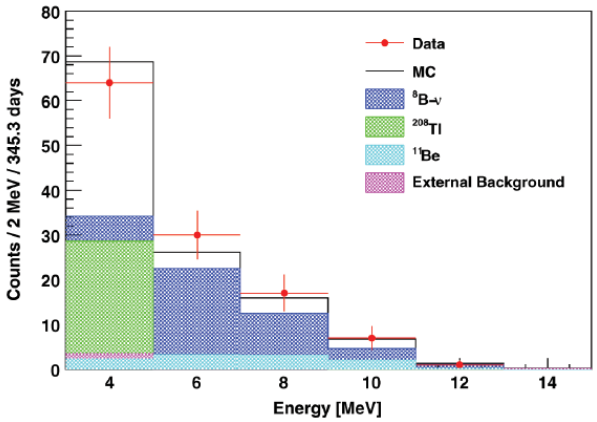

Fig. 16. The data (red) after all the cuts used in Borexino to extract the signal from the ^{8}B solar neutrino interaction rate together with the estimated amplitude of the residual background and the resulting signal.

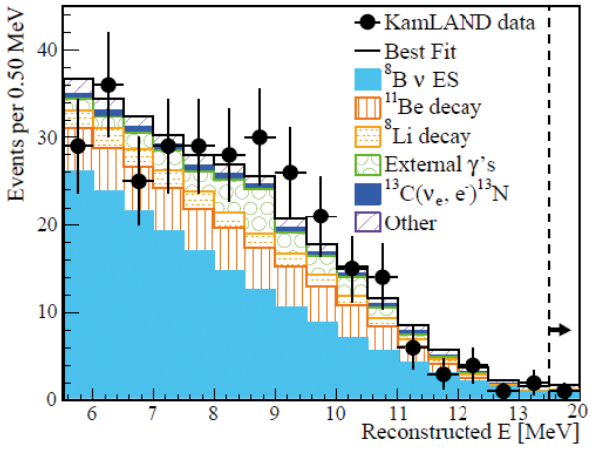

Fig. 17. Data of Kamland after the selection cuts used to get the signal from the ^{8}B solar neutrino interaction rate. The best fit obtained with a unbinned energy and rate analysis is shown.

vetoing all the detector for few seconds sec after a muon, When ^{10}C is produced in association with a neutron, ^{10}C candidates are tagged by the three-fold coincidence (TFC) with the parent muon and subsequent neutron capture in the scintillator similarly to what has been done for ^{11}C. The contribution of additional isotopes are studied through the time distribution of the events detected after a muon and close to the muon track as fig. 18 shows as

Table 6. Expected muon-induced contaminants with Q-value > 3 MeV in Borexino.

Isotopes	τ	Q [MeV]	Decay	Expected Rate [cpd/100 t]	Fraction > 3 MeV	Expected Rate > 3 MeV [cpd/100 t]	Measured Rate > 3 MeV [cpd/100 t]
^{12}B	0.03 s	13.4	β^-	1.41 ± 0.04	0.886	1.25 ± 0.03	1.48 ± 0.06
^{8}He	0.17 s	10.6	β^-	0.026 ± 0.012	0.898		
^{9}C	0.19 s	16.5	β^+	0.096 ± 0.031	0.965	$(1.8 \pm 0.3) \times 10^{-1}$	$(1.7 \pm 0.5) \times 10^{-1}$
^{9}Li	0.26 s	13.6	β^-	0.071 ± 0.005	0.932		
^{8}B	1.11 s	18.0	β^+	0.273 ± 0.062	0.938		
^{6}He	1.17 s	3.5	β^-	NA	0.009	$(6.0 \pm 0.8) \times 10^{-1}$	$(5.1 \pm 0.7) \times 10^{-1}$
^{8}Li	1.21 s	16.0	β^-	0.40 ± 0.07	0.875		
^{10}C	27.8 s	3.6	β^+	0.54 ± 0.04	0.012	$(6.5 \pm 0.5) \times 10^{-3}$	$(6.6 \pm 1.8) \times 10^{-3}$
^{11}Be	19.9 s	11.5	β^-	0.035 ± 0.006	0.902	$(3.2 \pm 0.5) \times 10^{-2}$	$(3.6 \pm 3.5) \times 10^{-2}$

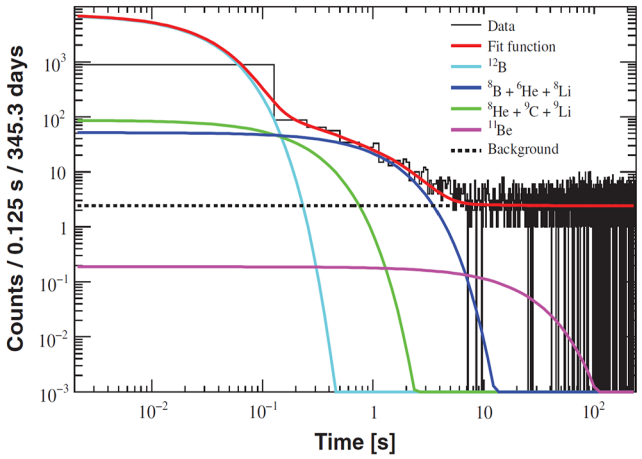

Fig. 18. Time profile of events in Borexino with energy $>$ 3 MeV within 240 s after a muon and within 2 m from its track in the entire Borexino active volume (278 t). The distribution has been fit to the three decay exponentials, plus the ^{11}Be component, with fixed mean lives.

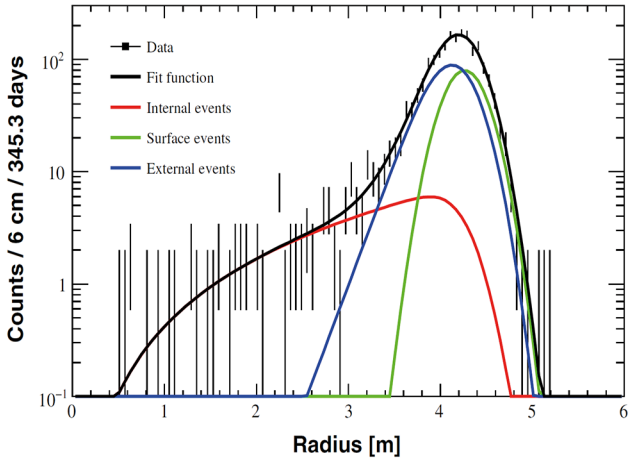

Fig. 19. Fit of the radial distribution of the Borexino events with energy > 3 MeV.

example. Additional possible sources are due to penetration of external γ in the fiducial volume, internal ^{214}Bi $\beta + \gamma$ decays ($Q = 3.27$ MeV), internal ^{208}Tl $\beta + \gamma$ decays ($Q = 5$ MeV).

The contribution of the external background is higher in Kamland than in Borexino mostly due to the different thickness of the water shield. Figure 19 shows the radial distribution of the events above 3 MeV in Borexino. Its study has established that the contribution of events from surface contamination and the exterior is negligible. The radial distribution of all scintillation events above 3 MeV has been fitted to a model which takes into account the three sources of backgrounds: a uniform distribution in the detector for internal events, a delta-function centered on the vessel radius for the point-like radioactive background in the nylon, and an exponential for external γ-ray background. The fit returns the amplitude of the three components.

In Kamland the external background has been studied with Monte Carlo simulations. It is mainly due to (n, γ) reactions in the surrounding rocks and in the stainless steel of the detector components. The simulation indicated that γ are attenuated exponentially with attenuation length of 53 ± 0.1 for rock and 53 ± 0.1 for stainless steel. Both values are in good agreement with the measured attenuation length obtained using data within 6 m radius.

9 Time variation analysis

The time variations of solar neutrinos have been studied by Borexino, specifically for the ^{7}Be component. Possible day-night changes have been studied in a fiducial volume larger (by a factor 1.75) than that used for the ^{7}Be flux measurement: in fact all the events reconstructed within a radius of 3.3 m have been used. The day and night spectra are built and then they are subtracted bin to bin; the residual spectrum is fitted with the ^{7}Be electron recoil spectrum. It is found that this method is more sensitive than a separate standard fit to the day and night spectra.

Also it allows to extend the fiducial region without introducing a detailed model for the background shape in the extended volume. The results are in [4] and [5].

The solar neutrino rate is expected to change during the year because of the variation of the distance between the Sun and the Earth. The detection of this modulation is a further signature (other then the spectral shape) of the solar origin of the neutrinos. As anticipated before, instead of using the spectral fit with time restricted data sample, different approaches have been used. They are based on the study of the time variation of the signals and they search for a component oscillating with one year period and the proper initial phase. The largest fiducial volume of Borexino has been used. It is based on the definition of the dynamical fiducial volume introduced in sect. 4. A 145 tons fiducial volume is obtained including all the events whose standoff distance from the measured, time-dependent surface of the vessel is 0.5 m. A new strong α-β cut has been introduced aiming to remove all the α events of ^{210}Po whose rate is not stable in time at the cost of the reduction of β events. Then the time variation of the count rate in the energy region dominated by the signal of ^{7}Be neutrinos is considered: it is the region defined by defined by $105 < N_{pe} < 380$. The relevant background is due to ^{85}Kr and ^{210}Bi. The modulated signal is searched by fitting the time binned data, by using the Lomb-Scargle method and by using the Empirical Mode Decomposition. All the three methods gave consistent results and they are detailed in [5]. The main issue is due to the time variation of the count rate of ^{210}Bi that reduces the sensitivity in the search for the small amplitude seasonal modulation.

10 Conclusion and future perspectives

The last component of the solar neutrino spectrum that still has to be measured is the CNO. Its flux is of primary importance both in the framewok of the Standard Solar Model and in astrophysics being the main fusione process powering stars with mass greater than the Sun. Borexino has provided the best limit. The main difficulty of the extraction of the CNO induced signal in liquid scintillator detectors is mainly related to the presence of ^{210}Bi: the similarity between the spectrum of its β decay and the recoil spectrum of electrons scattered by CNO neutrinos (see fig. 11) makes very hard the disentangling of the two components through a spectral fit. Appealing ideas about constraining the rate of ^{210}Bi on the basis of the rate of ^{210}Po have been proposed [24] and their feasibility in real experimental conditions have not yet been experimentally demonstrated. It is under study in Borexino. A purification campaign of the Borexino scintillator has allowed a further reduction of the internal background (particularly the ^{85}Kr) thus disclosing the possibility of measurements of the ^{7}Be and pep solar neutrino fluxes with increased accuracy.

In summary in this paper it has been reviewed how present days liquid scintillator based detectors have demonstrated the capability to detect very low-energy solar neutrinos probing almost all the solar neutrino energy spectrum. The procedures developed for the data analysis together with the intrinsic properties of liquid scintillators contributed to open the way toward the project of the next-generation large-volume detectors for low-energy neutrinos [25].

References

1. Borexino Collaboration (C. Arpesella *et al.*), Phys. Lett. B **658**, 101 (2008).
2. Borexino Collaboration (C. Arpesella *et al.*), Phys. Rev. Lett. **101**, 091302 (2008).
3. Borexino Collaboration (G. Bellini *et al.*), Phys. Rev. Lett. **107**, 141302 (2011).
4. Borexino Collaboration (G. Bellini *et al.*), Phys. Lett. B **707**, 22 (2012).
5. Borexino Collaboration (G. Bellini *et al.*), Phys. Rev. D **89**, 112007 (2014).
6. Borexino Collaboration (G. Bellini *et al.*), Phys. Rev. Lett. **108**, 051302 (2012).
7. Borexino Collaboration (G. Bellini *et al.*), Nature **512**, 383 (2014).
8. Borexino Collaboration (G. Bellini *et al.*), Phys. Rev. D **82**, 033006 (2010).
9. Kamland Collaboration (K. Eguchi *et al.*), Phys. Rev. Lett. **90**, 021802 (2003).
10. KamLAND Collaboration (A. Gando *et al.*), arXiv:1405.6190 (2014).
11. KamLAND Collaboration (S. Abe *et al.*), Phys. Rev. C **84**, 035804 (2011).
12. Borexino Collaboration (G. Alimonti *et al.*), Nucl. Instrum. Methods A **600**, 568 (2009).
13. F. Suekane *et al.*, arXiv:physics/0404071v2.
14. `http://kamland.lbl.gov/Dissertations/`.
15. Borexino Collaboration (H. Back *et al.*), JINST **7**, P10018 (2012).
16. Kamland Collaboration (B.E. Berger *et al.*), JINST **4**, P04017 (2009).
17. `thesis.library.caltech.edu/5946/1/Thesis_ChaoZhang_2010.pdf`.
18. `https://escholarship.org/uc/item/74f3c1nr` (T. O'Donnel phd thesis).
19. J.B. Birks, *The Theory and Practice of Scintillation Counting* (Macmillan, New York, 1964).
20. `kamland.lbl.gov/Dissertations/LindleyWinslow-DoctorThesis.pdf`.
21. KamLAND Collaboration (S. Abe *et al.*), Phys. Rev. C **81**, 025807 (2010).
22. Borexino Collaboration (G. Bellini *et al.*), JINST **6**, P05005 (2011).
23. D. Franco, G. Consolati, D. Trezzi, Phys. Rev. C **83**, 015504 (2011).
24. F. Villante *et al.*, Phys. Lett. B **701**, 336 (2011).
25. Yu-Feng Li, Int. J. Mod. Phys.: Conf. Ser. **31**, 1460300 (2014).